28. Ren, Y. & Zhang, F. C. Fermion analogy of anyon superconductivity in the two-dimensional electron gas. *Phys. Rev. B* **49,** 1532–1535 (1994).
29. Belitz, D. & Kirkpatrick, T. Are Si MOSFET's triplet superconductors. Preprint cond-mat/9705023 at ⟨http://xxx.lanl.gov⟩ (1997).
30. Zhitenev, N. B., Ashoori, R. C., Pfeiffer, L. N. & West, K. W. Periodic and aperiodic bunching in the addition spectra of quantum dots. *Phys. Rev. Lett.* **77,** 1833–1836 (1996).
31. Beasley, M. R., Mooij, J. E. & Orlando, T. P. Possibility of vortex-antivortex pair dissociation in two-dimensional superconductors. *Phys. Rev. Lett.* **42,** 1165–1168 (1979).
32. Moroni, S., Ceperley, D. & Senatore, G. in *Proc. Rochester Symp. on Strongly Coupled Plasmas* (eds van Horn, H. & Ichimaru, S.) 445–452 (Univ. Rochester Press, Rochester, 1993).

Acknowledgements. We thank B. Laughlin for comments on the presentation of this Letter, and thank E. Fradkin, N. Markovic, A. Goldman, A. Yazdani, A. Castro-Neto, A. Leggett, D. Ceperley, T. Giamarchi, P. Parris and S. Wan for discussions. This work was supported by the ACS Petroleum Research Fund and the NSF.

Correspondence and requests for materials should be addressed to P.P. (e-mail: dimer@uiuc.edu).

Laminated fabrication of polymeric photovoltaic diodes

M. Granström*, K. Petritsch*, A. C. Arias*, A. Lux†, M. R. Andersson‡ & R. H. Friend*

* *Cavendish Laboratory, Department of Physics, University of Cambridge, Madingley Road, Cambridge CB3 0HE, UK*
† *Cambridge Display Technology Ltd, 181A Huntingdon Road, Cambridge CB3 0DJ, UK*
‡ *Department of Polymer Technology, Chalmers University of Technology, S-412 96 Gothenburg, Sweden*

Photoexcited electron transfer between donor and acceptor molecular semiconductors provides a method of efficient charge generation following photoabsorption, which can be exploited in photovoltaic diodes[1–3]. But efficient charge separation and transport to collection electrodes is problematic, because the absorbed photons must be close to the donor–acceptor heterojunction, while at the same time good connectivity of the donor and acceptor materials to their respective electrodes is required. Mixtures of acceptor and donor semiconducting polymers[3,4] (or macromolecules[5]) can provide phase-separated structures which go some way to meeting this requirement, providing high photoconductive efficiencies. Here we describe two-layer polymer diodes, fabricated by a lamination technique followed by controlled annealing. The resulting structures provide good connectivity to the collection electrodes, and we achieve a short-circuit photovoltaic quantum efficiency of up to 29% at optimum wavelength, and an overall power conversion efficiency of 1.9% under a simulated solar spectrum. Given the convenience of polymer processing, these results indicate a promising avenue towards practical applications for such devices.

Applications involving conjugated polymers include light-emitting diodes, thin-film transistors, sensors and photovoltaic devices[6–10]. The last use the photovoltaic effect, by which electrons and holes are produced, and collected at electrodes when a semiconductor device is illuminated. In inorganic semiconductors, the photogenerated electrons and holes are free, whereas in the organic materials the absorption creates bound electron–hole pairs (excitons). These can be dissociated by the use of combinations of materials, one with small ionization potential and good hole-transport properties and the other with large electron affinity that acts as electron-transport material. This route has proven successful for organic photovoltaic devices, both as multilayer devices[11–13] and single-layer blend devices. The blends can be either polymer blends[3,4] or blends created by mixing molecular substances, such as C_{60} into a polymer matrix[5,14]. If this can be done so that a percolation path for the charge carrier is created, the efficiency of the devices is increased dramatically[15].

We use here a cyano derivative of poly(*p*-phenylene vinylene), MEH-CN-PPV (refs 16–18), as electron acceptor, and a derivative of polythiophene, POPT (refs 19–21), as hole acceptor. The structures of these are shown in Fig. 1a. The two polymers are soluble in chloroform or toluene, and are therefore conveniently mixed in solution. The structure of the laminated diodes is shown in Fig. 1b; these are assembled by forming a POPT-rich film on the ITO- or PEDOT-coated glass and an MEH-CN-PPV-rich film on the aluminium or calcium-coated glass substrate, and performing the lamination at an elevated temperature (here ITO is indium tin oxide; PEDOT is described in Fig. 1 legend).

If exciton splitting occurs in a blend of fluorescent polymers, it is usually faster than its radiative decay and can therefore be observed as photoluminescence (PL) quenching[3]. We measured the absolute PL efficiency using an integrating sphere as described previously[22], using excitation of wavelength 488 nm. In the MEH-CN-PPV/POPT blend, the PL is strongly quenched with only 5% or 10% of the thiophene polymer in the blend, dropping from 44% absolute PL efficiency for a pure MEH-CN-PPV film down to as low as 2%; this indicates efficient exciton dissociation in the blend. Energy

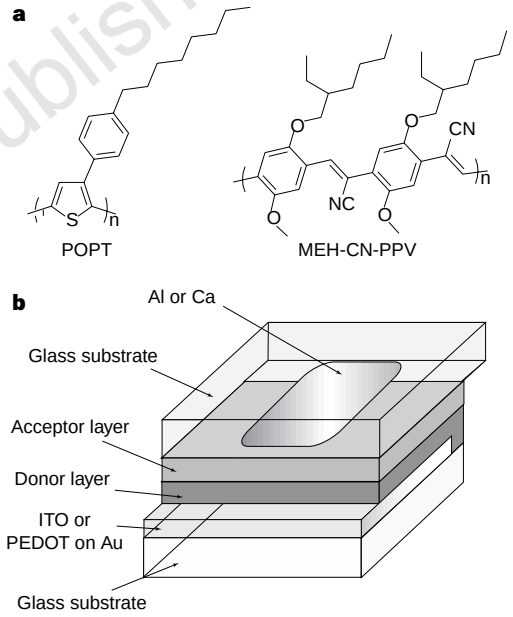

Figure 1 Chemical structures and device structure. **a**, Chemical structures of the polymers used in the devices. POPT is a regioregular phenyl-octyl substituted polythiophene which is found in two different forms[20,21] with the red-shifted structure obtained by thermal annealing of spin-coated films. This red-shifted form is preferred here as it provides the best match to the solar spectrum. MEH-CN-PPV is a fluorescent cyano-derivative of poly(*p*-phenylene vinylene), with a large electron affinity as a result of the electron-withdrawing cyano groups[16]. It and related polymers can be used as the emissive materials in efficient polymer light-emitting diodes[17,18]. **b**, Device structure. Both polymers (see **a** for chemical structures) were dissolved in chloroform or toluene (5 mg ml^{-1}) and the solutions were filtered with 0.45-μm filters before use. For the top half of the device, aluminium or calcium contacts were thermally evaporated ($P < 10^{-6}$ torr) on glass substrates, and the acceptor material, MEH-CN-PPV (and a small amount of POPT, usually 5%), was spin-coated on top of the metal electrode. The other half of the device comprises the donor material, POPT (and a small amount of MEH-CN-PPV, usually 5%), spin-coated on either ITO substrates or glass coated with poly(ethylene dioxythiophene) doped with polystyrene sulphonic acid (PEDOT:PSS, Bayer AG, Ludwigshafen, Germany). To ensure a low contact resistance, a thin layer of gold (~10 nm) was thermally evaporated on the glass slide before spin-coating the PEDOT film from a water solution. The thickness of the PEDOT layer was 100 nm. To get the desired structure of the POPT[19], this half of the device was heated to 200 °C under vacuum before the device was laminated together by applying a light pressure while one half was still at elevated temperature. The total thickness of the organic semiconductive layer was 70–80 nm, and the active area 2.5 mm^2.

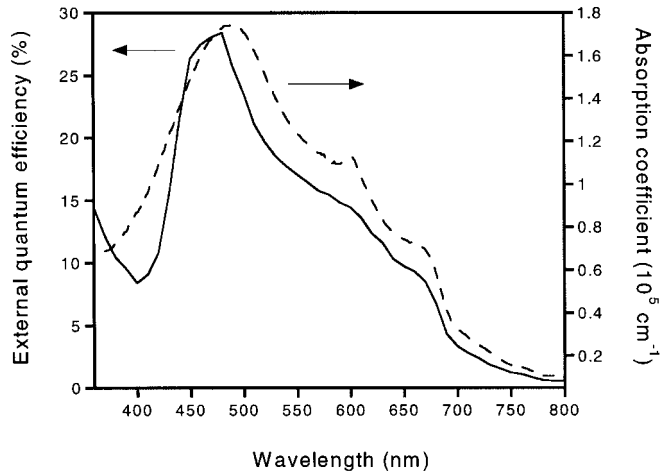

Figure 2 Optical properties. Shown are the optical absorption, measured as –log(transmittance), of a POPT/MEH-CN-PPV double layer (dashed line) and external quantum efficiency of an ITO/POPT:MEH-CN-PPV (19:1)/MEH-CN-PPV:POPT (19:1)/Al device (solid line). Measurements of photocurrent were made by illuminating the samples from the ITO or PEDOT side with a tungsten–halogen lamp, dispersed by a Bentham M300 single-grating monochromator. Electrical data were measured and bias voltage was applied using a Keithley 237 source-measure unit. Absorption spectra were measured with a Hewlett Packard 8453 ultraviolet–visible spectrometer.

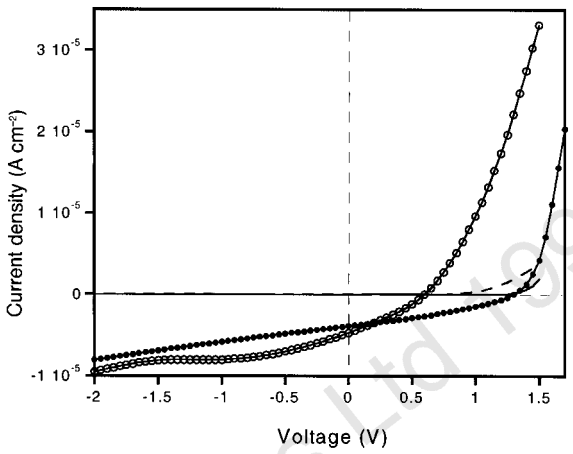

Figure 3 Current–voltage characteristics. Data shown are for laminated double-layer devices using POPT:MEH-CN-PPV (19:1)/MEH-CN-PPV:POPT (19:1) blends. Open circles and dashed line show light (480 nm, 34 μW cm^{-2}) and dark current for a device with ITO and Al as electrodes (open-circuit voltage 0.6 V), whereas the filled circles and solid line show the response in light and darkness for a device with PEDOT and Ca as electrode materials (open-circuit voltage 1.3 V). The characteristics were measured in the dark, and using narrow lines from the monochromator.

transfer to the blending partner as an alternative explanation is ruled out because the PL of both materials is quenched in the blend.

As a starting point, we made single-layer blend devices, similar to those previously reported[3,4], from the MEH-CN-PPV/POPT blends. This was done with non-heated films, resulting in devices with external quantum efficiencies of the order of 3–5%, which is comparable to other polymer blend devices. However, because POPT needs to be heated (or solvent-treated) to reach the ordered state which has its absorption in the long-wavelength range, the phase-separation properties become less favourable. Because of the heating, not only do the POPT chains themselves have a chance to relax and find a more ordered state, so does the blend as a whole. This results in a phase separation on a much larger length scale than preferred (about 200–400 nm, as seen in atomic force microscopy (AFM) images), which radically decreases the external quantum efficiency down to about 0.05%, a value comparable to the result for single-layer MEH-CN-PPV devices.

We developed the device structures using laminated double-layer arrangements (Fig. 1b). In this way, it is possible to reach the desired coverage of the wavelength range, and, simultaneously, make sure that the acceptor material has a proper contact with the low-work-function contact (Al or Ca) and the donor with the high-work-function contact (ITO or PEDOT). Simple laminated devices with two homolayers were found to have the desired wavelength response, but not particularly high efficiencies, albeit somewhat higher than the single-layer blend devices. But, by adding a small amount of POPT to the MEH-CN-PPV layer, 2–5 wt%, the efficiency of the devices was much increased compared to the double-layer device or single-layer blend. The external quantum efficiency follows the absorption (Fig. 2), suggesting that there is no inactive layer which would act as an optical filter and thereby decrease the efficiency. At −1 V and −2 V the curve (not shown) is slightly shifted towards shorter wavelengths, and the efficiencies at 480 nm are 49% and 58%, respectively. The addition of a similar small amount of MEH-CN-PPV to the POPT layer did not make any significant difference to the device efficiency, most probably because of phase-separation changes caused by heating the film.

Figure 3 shows the current–voltage response of the device, measured in darkness and excited at 480 nm. A distinct diode behaviour is found, and the rectification ratio in the dark is $>10^3$ at ± 1.5 V. The fill factor, FF, is defined as the maximum power $(IV)_{max}$ that can be extracted from a photovoltaic diode divided by the product of maximum current I_{sc} and maximum voltage V_{oc}:

$$\mathrm{FF} = \frac{(IV)_{\max}}{I_{\mathrm{sc}} V_{\mathrm{oc}}} \tag{1}$$

Using this definition, we get values in the range of 30–35% for both types of devices described above (single-layer blend and laminated double-layer blend). The power conversion efficiency η_P is defined as the ratio of the input power P_{in}, in the form of electromagnetic radiation, to the output power P_{out} in the form of electrical energy:

$$\eta_{\mathrm{P}} = \frac{P_{\mathrm{out}}}{P_{\mathrm{in}}} = \frac{(IV)_{\max}}{LA} \tag{2}$$

where L is the intensity of the illumination, and A is the active area. When the fill factor is known, equation (2) translates into:

$$\eta_{\mathrm{P}} = FF\frac{I_{\mathrm{sc}} V_{\mathrm{oc}}}{LA} \tag{3}$$

Open-circuit voltage can be selected by choice of the work functions of the electron- and hole-accepting electrodes. We have maximized this for an Au/PEDOT/POPT:MEH-CN-PPV (19:1)/MEH-CN-PPV:POPT (19:1)/Ca device, for which the current–voltage characteristics are shown, together with those for a device made with ITO and Al electrodes, in Fig. 3. The spectral response is very similar for both devices. For the Au/PEDOT and Ca electrode device, the external quantum efficiency reaches 29% with 480 nm excitation and no applied bias. Calculating the power conversion efficiency using these values then gives $\eta_P = 4.8\%$ at the peak wavelength, rising to ~7% at solar illumination intensities, which is a significant increase compared to previous polymer devices. We calculate a power conversion efficiency for a simulated solar spectrum, AM 1.5 (77 mW cm^{-2}) of 1.9%. Under 2 V negative bias, this device has a quantum efficiency of 61% at the peak wavelength. The dependence of open-circuit voltage and short-circuit current on the intensity of incident light L (at 488 nm) is shown in Fig. 4. The short-circuit current is very close to linear ($I_{sc} \propto L^{1.02}$) up to the highest value measured here of 100 mA cm^{-2}, whereas the open-circuit voltage

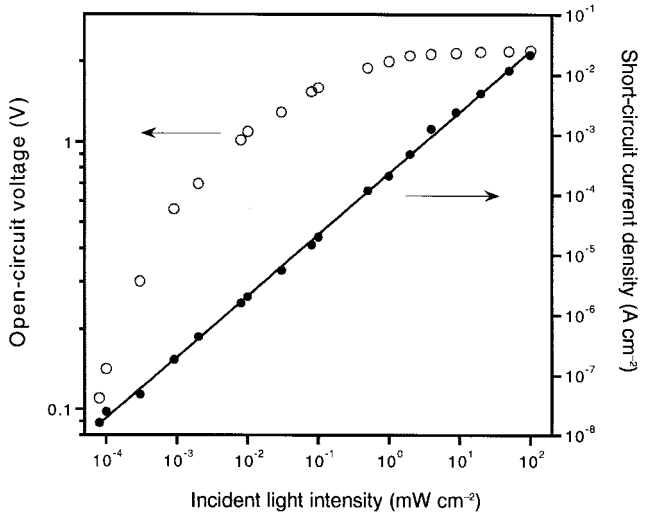

Figure 4 Effect of light intensity. Shown are the dependence of open-circuit voltage (open circles) and short-circuit current density (filled circles) of an Au/PEDOT/POPT:MEH-CN-PPV (19:1)/MEH-CN-PPV:POPT (19:1)/Ca device on incident light intensity. The device was illuminated using the 488-nm line from an argon-ion laser. The fill factor, as defined in equation (1), is relatively constant, ranging from 0.30 to 0.34.

increases sublinearly with intensity, saturating when the value approaches 2.2 V, which is close to the estimated difference in work function between the two electrodes.

We used tapping-mode AFM to investigate the structure of these devices. This technique has been found previously to give good contrast between different polymers[23], and we find here that better contrast is obtained using phase-detection (which provides a measure of the viscoelasticity). Figure 5a and b shows the in-plane structures of the MEH-CN-PPV-rich layer and the POPT-rich layers, respectively. We note clear evidence for formation of 'islands' of the minority phase, which are larger in size for the heat-treated POPT-rich film. Figure 5c shows the cross-section of a laminated structure: there is interpenetration between the two layers following the lamination and annealing procedure, with a length scale of 20–30 nm. We note that finer-scale interpenetration is not expected to be revealed in these AFM images.

There is increased interest in solar energy conversion, though cost per installed kilowatt for inorganic semiconductor devices remains high, and there is renewed interest in the development of novel photovoltaic cells. These include photoelectrochemical cells which use dye adsorbed onto sintered titanium dioxide, which show high solar energy conversion efficiencies[24] and which are under active development. The devices which we have developed now show quantum efficiencies which approach usable values; they also have several desirable practical attributes such as low-temperature processing which is compatible with fabrication onto polymer substrates, which offers low-cost large-area manufacture. Our devices have good efficiency, especially at high illumination levels (Fig. 4), which is achieved in spite of low carrier mobilities because the total semiconductor film thickness is very small (100 nm here). We also comment that the devices which we report here show efficient operation over the full visible spectrum, and, by virtue of the absorption spectrum of the POPT, even extends into the infrared region. Further development is required to match better the solar spectrum. □

Received 6 April; accepted 19 June 1998.

1. Tang, C. W. Two-layer organic photovoltaic cell. *Appl. Phys. Lett.* **48,** 183–185 (1986).
2. Halls, J. J. M., Pichler, K., Friend, R. H., Moratti, S. C. & Holmes, A. B. Exciton diffusion and dissociation in a poly(p-phenylenevinylene)/C_{60} heterojunction photovoltaic cell. *Appl. Phys. Lett.* **68,** 3120–3122 (1996).

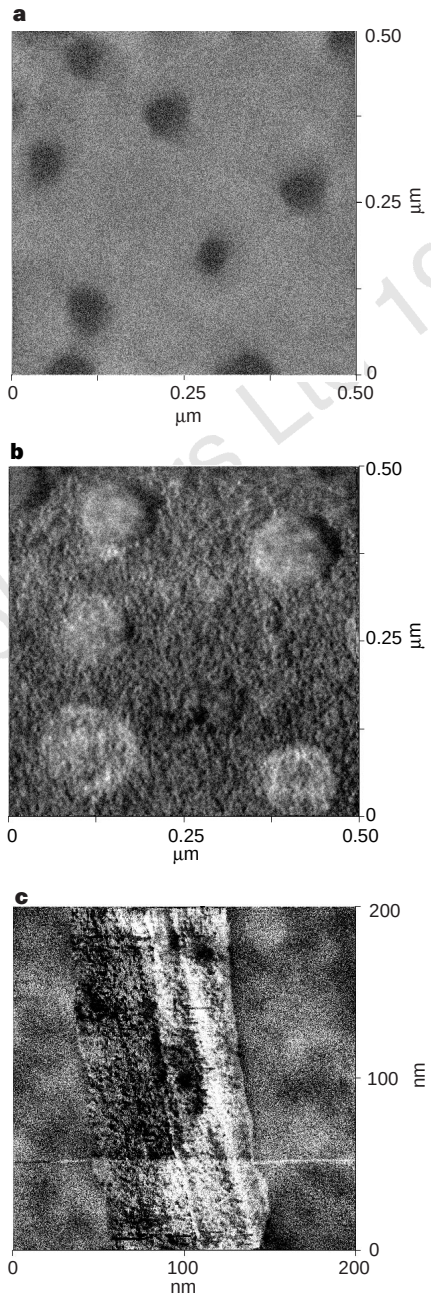

Figure 5 Tapping-mode AFM images. **a**, An in-plane image of MEH-CN-PPV:POPT (19:1). **b**, An in-plane image of annealed POPT:MEH-CN-PPV (19:1). The images are shown in phase contrast, most of which is due to differences in viscoelastic properties of the two polymers; height differences are no more than 5 nm. **c**, A cross-sectional image, obtained for a structure formed without metal electrodes and with polyester substrates (the cut to reveal the cross-section was made at low temperature). Images were obtained using phase-sensitive detection, and were taken using a NanoScope IIIa Dimension 3100 (Digital Instruments Inc, Santa Barbara).

3. Halls, J. J. M. *et al.* Efficient photodiodes from interpenetrating polymer networks. *Nature* **376,** 498–500 (1995).
4. Yu, G. & Heeger, A. J. Charge separation and photovoltaic conversion in polymer composites with internal donor-acceptor heterojunctions. *J. Appl. Phys.* **78,** 4510–4515 (1995).
5. Yu, G., Gao, J., Hummelen, J. C., Wudl, F. & Heeger, A. J. Polymer photovoltaic cells-enhanced efficiencies via a network of internal donor-acceptor heterojunctions. *Science* **270,** 1789–1791 (1995).
6. Burroughes, J. H. *et al.* Light-emitting diodes based on conjugated polymers. *Nature* **347,** 539–541 (1990).
7. Willander, M., Assadi, A. & Svensson, C. Polymer-based devices their function and characterization. *Synth. Met.* **57,** 4099–4104 (1993).
8. Partridge, A. C., Harris, P. & Andrews, M. K. High-sensitivity conducting polymer sensors. *Analyst* **121,** 1349–1353 (1996).

9. Yu, G. & Heeger, A. J. High efficiency photonic devices made with semiconducting polymers. *Synth. Met.* **85,** 1183–1186 (1987).
10. Friend, R. H. *et al.* Electronic excitations in luminescent conjugated polymers. *Solid State Commun.* **102,** 249–258 (1997).
11. Tada, K., Onoda, M., Zakhidov, A. A. & Yoshino, K. Characteristics of poly(p-pyridyl vinylene)/poly(3-alkylthiophene) heterojunction photocell. *Jpn. J. Appl. Phys. Pt2-Lett.* **36,** L306–L309 (1997).
12. Takahashi, K. *et al.* Enhanced quantum yield in porphyrin/electron-donor double-layer solar cells. *Solar Energy Mater. Solar Cells* **45,** 127–139 (1997).
13. Yoshino, K., Tada, K., Fujii, A., Conwell, E. M. & Zakhidov, A. A. Novel photovoltaic devices based on donor-acceptor molecular and conducting polymer systems. *IEEE Trans. Electron. Devices* **44,** 1315–1324 (1997).
14. Roman, L. S., Andersson, M. R., Yohannes, T. & Inganäs, O. Photodiode performance and nanostructure of poly(thiophene)/C_{60} blends. *Adv. Mater.* **9,** 1164–1168 (1997).
15. Yang, C. Y. & Heeger, A. J. Morphology of composites of semiconducting polymers mixed with C_{60}. *Synth. Met.* **83,** 85–88 (1996).
16. Moratti, S. C. *et al.* High electron-affinity polymers for LEDs. *Synth. Met.* **71,** 2117–2120 (1995).
17. Greenham, N. C., Moratti, S. C., Bradley, D. D. C., Friend, R. H. & Holmes, A. B. Efficient polymer-based light-emitting diodes based on polymers with high electron affinities. *Nature* **365,** 628–630 (1993).
18. Baigent, D. R. *et al.* Light-emitting diodes fabricated with conjugated polymers—recent progress. *Synth. Met.* **67,** 3–10 (1994).
19. Andersson, M. R. *et al.* Electroluminescence from substituted poly(thiophenes)—from blue to near-infrared. *Macromolecules* **28,** 7525–7529 (1995).
20. Berggren, M. *et al.* Thermal control of near-infrared and visible electroluminescence in alkyl-phenyl substituted polythiophenes. *Appl. Phys. Lett.* **65,** 1489–1491 (1994).
21. Andersson, M. R. *et al.* Regioselective polymerization of 3-(4-octylphenyl)thiophene with $FeCl_3$. *Macromolecules* **27,** 6503–6506 (1994).
22. de Mello, J. C., Wittmann, H. F. & Friend, R. H. An improved experimental determination of external photoluminescence quantum efficiency. *Adv. Mater.* **9,** 230–232 (1997).
23. Granström, M. *et al.* Self-organizing polymer films—a route to novel electronic devices based on conjugated polymers. *Supramol. Sci.* **4,** 27–34 (1997).
24. O'Regan, B. & Grätzel, M. A low-cost, high-efficiency solar cell based on dye-sensitized colloidal TiO_2 films. *Nature* **353,** 737–740 (1991).

Acknowledgements. Financial support from the Engineering and Physical Sciences Research Council, the European Commission (TMR Marie Curie fellowship and TMR Network SELOA), and from CNPq, Brazilian government, is gratefully acknowledged.

Correspondence and requests for materials should be addressed to R.H.F. (e-mail: rhf10@cam.ac.uk).

RNA-catalysed nucleotide synthesis

Peter J. Unrau & David P. Bartel

Whitehead Institute for Biomedical Research, and Department of Biology, MIT, 9 Cambridge Center, Cambridge, Massachusetts 02142, USA

The 'RNA world' hypothesis proposes that early life developed by making use of RNA molecules, rather than proteins, to catalyse the synthesis of important biological molecules[1]. It is thought, however, that the nucleotides constituting RNA were scarce on early Earth[1–4]. RNA-based life must therefore have acquired the ability to synthesize RNA nucleotides from simpler and more readily available precursors, such as sugars and bases. Plausible prebiotic synthesis routes have been proposed for sugars[5], sugar phosphates[6] and the four RNA bases[7–11], but the coupling of these molecules into nucleotides, specifically pyrimidine nucleotides, poses a challenge to the RNA world hypothesis[1–3]. Here we report the application of *in vitro* selection to isolate RNA molecules that catalyse the synthesis of a pyrimidine nucleotide at their 3′ terminus. The finding that RNA can catalyse this type of reaction, which is modelled after pyrimidine synthesis in contemporary metabolism, supports the idea of an RNA world that included nucleotide synthesis and other metabolic pathways mediated by ribozymes.

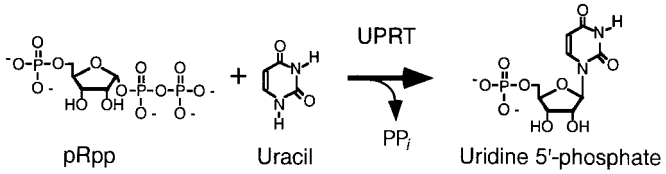

Figure 1 UPRT-catalysed synthesis of uridine 5′-phosphate from pRpp and uracil.

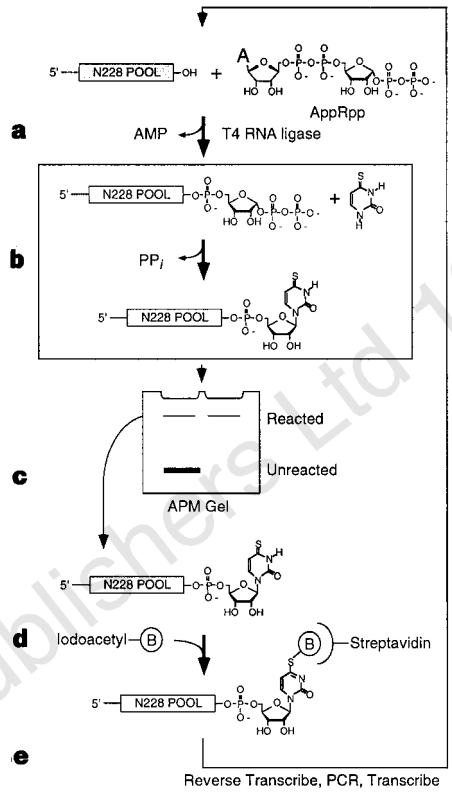

Figure 2 *In vitro* selection scheme. Symbols: PP$_i$, pyrophosphate; B, biotin. **a**, Tethering pool RNA to pRpp by using T4 RNA ligase and adenylylated pRpp (AppRpp). **b**, ^{4S}U synthesis promoted by active sequences within the initial pool. **c**, Enrichment of reacted sequences by using APM gels. One lane (left) contained radiolabelled pool RNA. The other lane (right) contained radiolabelled synthetic standard to mark the location of the reacted RNA. After the first round of selection, catalysts were enriched by serial purification on two APM gels. **d**, Further enrichment of ^{4S}U-containing sequences by derivation with iodoacetyl-LC-biotin (Pierce) and capture with streptavidin magnetic beads. **e**, Amplification of enriched RNA by reverse transcription, PCR and transcription. The amplified RNA was then subjected to another round of selection *in vitro*.

In modern metabolism, pyrimidine nucleotides are synthesized from activated ribose (pRpp) and pyrimidine bases (such as uracil or orotate). For example, uracil phosphoribosyltransferase (UPRT) catalyses the reaction shown in Fig. 1. The chemistry of this reaction, nucleophilic attack on carbon after release of pyrophosphate, is central to the biosynthesis of nucleotides and amino acids (histidine and tryptophan), yet absent from known ribozyme reactions. The reaction differs from known RNA-catalysed reactions in other key respects: it occurs by an S_N1 mechanism (involving the stabilization of an oxocarbocation at the reaction centre, C1′ of ribose)[12,13], and uracil is significantly smaller than the smallest ribozyme substrates.

To explore the ability of RNA to promote nucleotide synthesis, we performed an iterative selection *in vitro* to isolate from random sequences ribozymes that synthesized a pyrimidine nucleotide at their 3′ terminus (Fig. 2). The initial pool of sequences contained $> 1.5 \times 10^{15}$ different RNA molecules, each with 228 random positions. To begin each selective round, pRpp was attached to the 3′ end of pool RNA. RNA-pRpp conjugates were incubated with a uracil analogue, 4-thiouracil (^{4S}Ura), to allow those sequences capable of glycosidic bond formation the opportunity to link their tethered ribose to ^{4S}Ura. RNAs attached to the newly synthesized nucleotide, 4-thiouridine (^{4S}U), were then enriched, amplified, and subjected to another round of selection–amplification. ^{4S}U was chosen as the desired product because the thione at position 4